Europium-Doped $Ba_7F_{12}Cl_2$, a Single Component Near-UV Excited Tunable White Phosphor

Hans Hagemann,*,[†] Hans Bill,[†] Julien M. Rey,[†,‡] Frank Kubel,[§] Laurent Calame,[||] and Dominique Lovy[†]

[†]Dépt. de Chimie Physique, Univ. de Genève, 30, q. E. Ansermet, CH 1211 Geneva 4 Switzerland

[§]Inst. für Chemische Technologien und Analytik, TU Wien, Getreidemarkt 9/164 SC, A1060 Vienna, Austria

[||]Institut de Micro et Nano Techniques (MNT), Haute Ecole d'Ingénieurs et de Gestion du Canton de Vaud (HEIG-VD) HES-SO, Av. des Sports 14, CH-1400 Yverdon-les-Bains Switzerland

Ⓢ Supporting Information

ABSTRACT: Europium-doped crystalline $Ba_7F_{12}Cl_2$ phosphors have been prepared at temperatures between 650 and 900 °C using alkali chloride fluxes, yielding both disordered (with the incorporation of small amounts of Na) and ordered crystal modifications. The white emission spectrum excited in the near UV consists roughly of two broad emission bands at about 450 and 590 nm, as well as weak sharp Eu^{2+} 4f−4f emission bands around 360 nm. The incorporation of Eu^{2+} is further studied using EPR spectroscopy on single crystals and reveals a significant zero field splitting. The emission spectrum can be significantly tuned by varying the excitation wavelength between 300 and 390 nm. Fine tuning may also be achieved by chemical substitutions to form $Ba_{7-x}M_yF_{12}Cl_{2-z}Br_z$ (M = Na, Ca, Eu). Quantitative measurements of the light produced using commercial near UV LEDs show that the color temperature ranges between 4000 and 9700 K with CIE chromaticity coordinates close to the ideal values of $x = y = 0.333$. The best color rendering index (CRI) found was 0.83 and the highest light to light conversion yield was 171 lm/W. These results show that the title compound is a very promising candidate for white light generation using near UV LED excitation.

homogeneous single crystal (~0.4mm) of $Ba_7^{[Eu(II,III)]}F_{12}Cl_2$ exitation at 254nm
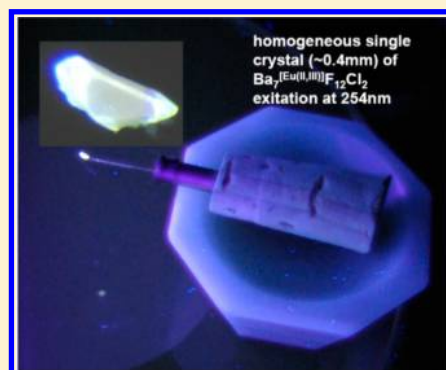
■ INTRODUCTION

Light-emitting diodes (LED) are very energy efficient light sources compared to incandescent and fluorescent lamps.[1] However, in order to obtain white light emission, a phosphor layer must be added to expand the spectral range of the emitted light. The requirements for a good white phosphor material are CIE (International commission on Illumination) coordinates of $x = 0.333$ and $y = 0.333$, a color temperature (CCT) in the range of 2500−6500 K and a color rendering index (CRI) above 80.[2]

Typically, a combination of rare earth ions (e.g., Ce^{3+} + Tb^{3+})[3] or rare earth ions and transition metals (e.g., Eu^{2+} + Mn^{2+})[4−6] or only transition metals[7] are used to generate white light by the addition of the respective emission spectra. It is difficult to achieve a good CRI index; for this reason, some phosphors contain three rare earth ions such as Dy^{3+}-, Tb^{3+}-, and Eu^{3+}-doped $LaPO_4$[8] or Tm^{3+}-, Tb^{3+}-, and Eu^{3+}-doped LaF_3 nanoparticles.[9] Ce^{3+}, Mn^{2+}, and Tb^{3+} codoped phosphors have also been reported.[10]

In this work, we present a single compound near-UV excited tunable white phosphor material, which requires only one dopant rare earth ion, namely, Eu^{2+}. Eu^{2+}-doped $Ba_7F_{12}Cl_2$ is easy to prepare and is stable up to 800 °C. It is stable for years under ambient conditions and is only slightly soluble in water. The spectroscopic properties of this material are presented, and the performance as potential white phosphor material is demonstrated.

Structural and Chemical Properties of $Ba_7F_{12}Cl_2$. $Ba_7F_{12}Cl_2$ can be obtained in two crystalline modifications, an ordered (with space group $P\bar{6}$) and a disordered (with space group $P6_3/m$).[11,12] In the ordered modification, there are three different Ba sites (which can potentially be substituted by Eu), while in the disordered modification there are only two different Ba sites (see Figures S1 and S2). The disordered modification is stabilized by the presence of small amounts of Na.[13] The crystal structure can further be modulated (Figure S3) by chemical substitutions for instance when partially replacing Ba by Ca and Cl by Br.[14−16] Several methods are available to obtain these $Ba_{7-x}M_yF_{12}Cl_{2-z}Br_z$ compounds (M = Na, Ca, Eu) with $x,y \leq 1$, $0 \leq z \leq 2$,[11−17] such as direct solid state reaction of the two binaries BaF_2, $BaCl_2$, or flux dissolution of BaF_2 in alkali fluorides/chlorides. This latter method allows to obtain needle-shaped single crystals.

Initially, needles of $Ba_7F_{12}Cl_2$ had been obtained in our Bridgman crystal growth equipment (Figure S4).

■ EXPERIMENTAL SECTION

Synthesis. Crystals of $Ba_7F_{12}Cl_2$ have been prepared from the melt of mixtures of alkali halides and BaF_2.

The disordered modification was typically obtained starting from 8 g BaF_2 + 1.77 g of NaCl. EuF_3 (typically less than 1 mol % with respect to Ba) was added. The reaction mixtures were heated in graphite crucibles under a nitrogen atmosphere up to 950 °C and slowly cooled (in 14 h) to 750 °C before cooling to room temperature. The resulting products showed the presence of needle-shaped crystals. Washing with warm water removed most of the remaining alkali halide flux material. This procedure yields about 90% pure phosphor, with mainly BaF_2 as impurity.

The ordered modification is obtained either from BaF_2 and LiCl, or BaF_2 and LiCl + KCl; however, the resulting solid contains also significant amounts of $LiBaF_3$. Needle-shaped single crystals of $Ba_7F_{12}Cl_2$ can nevertheless be separated mechanically from the solidified melt. A typical size of the single crystals obtained was $0.15 \times 0.15 \times 3 \ mm^3$. The ordered modification can also be obtained by heating the disordered modification (prepared as above) to 800 °C.[13]

The typical procedure to synthesize the ordered modification with the crystal growth equipment under thoroughly controlled conditions was as follows. Purest available BaF_2 (Merck Suprapur, 99.99% pure), $BaCl_2$ (99.995% pure), and $EuCl_2$ and EuF_2 (both Cerac, certified purity 99.9%) were beforehand degassed in a high vacuum line including a coldfinger at −196 °C. The temperature was stepwise increased from RT to T = 140 °C. Typical batches of 45 g total weight were prepared and filled into an ultrapure carbon crucible (Le Carbone nuclear purity) in a glovebox (8 ppm residual O_2 content). The stoichiometric mixture included 0.1−2 mol % of EuF_2 + $EuCl_2$. The batch was introduced into the furnace and degassed under high vacuum for approximately 12 h with a liquid nitrogen trap (T = −196 °C) connected, while heating slowly up to 240 °C. The solid state reaction was initiated after Ar (6N; in some runs, +0.2% H_2 (6N)) had been entered into the chamber containing the crucible. The temperature was then increased to about 805 °C. After about 26 h at this temperature, the heater was switched off. This reaction cycle was repeated twice. Between two cycles, the content of the crucible was ground for 1 min in the glovebox using an agate mortar. The ordered luminophor $Ba_7F_{12}Cl_2$ was obtained with a purity of more than 96.8%.

This furnace (Figure S4) and a Kyropoulos equipment served further for a quantitative production (totally ca. 1 kg of the product) of ordered $Ba_7F_{12}Cl_2$ under very thoroughly controlled conditions.

The samples used for the EPR experiments were oriented with the aid of a polarizing microscope and by the Laue X-ray technique.

Spectroscopic Experiments. *Optical Measurements.* Luminescence and optical excitation measurements at medium resolution were carried out with a home-built spectropho-tometer[18,19] as well as with a Fluorolog F 3−22 instrument.

For optical measurements at high resolution, the excitation setup consisted of a xenon lamp (500 W, ILC Tech.) and a monochromator (H20, ISA). The luminescence was analyzed with a monochromator (SPEX 1403). The detection consisted in a cooled (≈−40 °C) photomultiplier (Burleigh C31034-A20), followed by a discriminator (Hamamatsu C3866) and a photon-counting unit (SR400, Stanford Research). Part of the excitation light was redirected on a photodiode (Hamamatsu S1226) in order to correct the spectra for the intensity variation of the Xe lamp.

The luminescence decays were measured after excitation with a nitrogen laser (KX2, Oxford Laser, pulse length < 20 ns,

wavelength 337.1 nm). A photodiode (Hamamatsu, S5973) with a frequency cutoff of 1.5 GHz was used to trigger the decay. The emission was analyzed with a Cary14 mono-chromator and two types of detectors were used, a photodiode (Hamamatsu S3883, frequency cutoff 300 MHz) and a photomultiplier (Hamamatsu H6240−01). The signals were collected and averaged with a digital oscilloscope (LeCroy 9420, bandwidth 0−350 MHz).

EPR. The EPR spectra were obtained at 36 GHz on a home-built Ka-band spectrometer with low-temperature equipment of our design. Data analysis and computer simulations were performed with our SPINHAM program.[18,19]

Prototype White Light Generation Using Commercial UV LEDs. Several quantitative experiments of white light generation were performed with two consecutively improved set-ups. The second one is illustrated in Figure S5: The LED is placed below the sample, which consists of the phosphor material (with a silicone binder), and the system is covered by an integrating sphere. This setup allows to control accurately the thickness of the tested phosphor layer.

■ RESULTS AND DISCUSSION

Figure 1 presents typical emission and excitation spectra of disordered $Ba_7F_{12}Cl_2$:Eu^{2+} at room temperature. These spectra
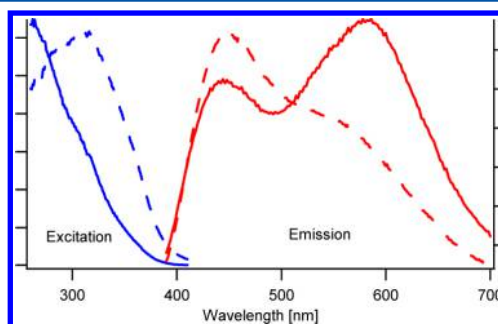
Figure 1. Emission spectra excited at 340 nm (red traces) and excitation spectra monitored at 580 nm (blue traces) for disordered $Ba_7F_{12}Cl_2$:Eu^{2+} (full line) and the ordered form (dashed line) at 300 K.

consist basically of two broad bands that cover a very large part of the visible spectrum.

The 80K emission spectra (excited at 280 nm) for ordered $Ba_7F_{12}Cl_2$ are presented in Figure 2. They exhibit several
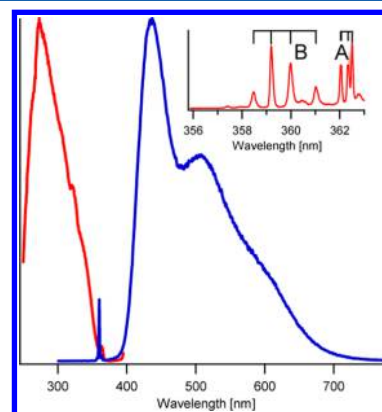

Figure 2. Emission (excited at 280 nm) and excitation (detected at 410 nm) spectra of ordered $Ba_7F_{12}Cl_2$:Eu at 80 K. The inset represents an enlargement of the f−f emissions with a better resolution.

unresolved $4f^6 5d^1 \rightarrow 4f^7$ bands covering the entire visible spectrum. The emission of the ordered form shows three emission band with maxima at 437 nm (22900 cm^{-1}), 510 nm (19600 cm^{-1}), and about 595 nm (16800 cm^{-1}; see Table 1).

Table 1. Positions of the $f-f$ Lines (Top Lines) and $f-d$ Maxima (Bottom Lines) Emission for the Ordered $Ba_7F_{12}Cl_2$:Eu $(1°/_0)$ at 80 and 10 K

site	T (K)	position (cm^{-1})
A	80	27′624 27′621 27′600 27′588
A	10	27′600 27′588
B	80	27′898 27′843 27′782 27′700
B	10	27′844 27′786 27′704
$f-d$	80	22′900 19′600 ca. 16′800
$f-d$	10	22′700 19′400 ca. 16′500

The excitation spectrum at 80K (detected at 410 nm; Figure 2) consists of large features also formed by several unresolved bands. Lowering the temperature to 10 K decreases the width of the emitted bands and allows to obtain the excitation spectrum of the individual band (Figure S6). Each band has a different excitation spectrum but all of them are confined between 40000 and 26000 cm^{-1}, as illustrated also by the room temperature transmittance spectrum of a single crystal of ordered $Ba_7F_{12}Cl_2$ doped nominally with 0.5% of Eu^{2+} in Figure 3 (as well as in Figure S7, which shows an absorption spectrum
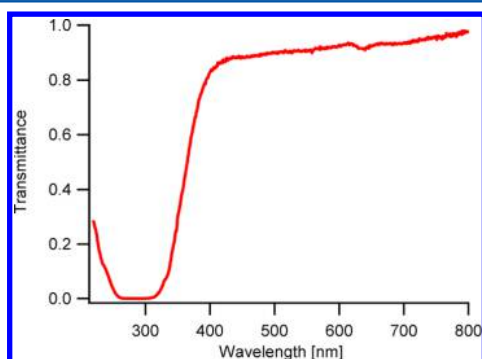
**Figure 3.** Room temperature absorption spectrum of a single crystal of ordered $Ba_7F_{12}Cl_2$:Eu.

measured on a film prepared with the ordered modification dispersed with ethylcellulose). The thickness of this crystal was about 0.25 mm. At 365 nm, the transmittance is about 50%.

Both the emission and excitation spectra show narrow lines due to 4f–4f ($f-f$) transitions of the Eu^{2+} at 80 K. A high resolution spectrum of the 4f–4f emission in the $Ba_7F_{12}Cl_2$:Eu (ordered) is presented in the inset of Figure 2. The lines can be separated into two groups with the aid of their excitation spectra. The first group (A) has three resolved lines. A careful analysis showed that one of them is broader and contains two unresolved lines. The second group (B) has four lines with a stronger splitting. The position of each line is given in Table 1. As can be seen from the values in Table 1, the successive separations of the sublevels are quite irregular, as can be expected for a low local symmetry of the Eu^{2+} ion.[20]

Decay times of the emission in the ordered and disordered forms are very similar. At 80 K after excitation at 29660 cm^{-1}, the decay is not single exponential, and the form of the decay varies with the position of the detection. In the high-energy part of the emission spectrum, the decay is fast (≈ 0.8 μs at 23500

cm^{-1}) and becomes longer when the detection is moved to the low energy part (≈ 2 μs at 16500 cm^{-1}). At room temperature, the decay times are only slightly shorter, indicating also that the emission quantum yield is quite high. Figure 4 shows the
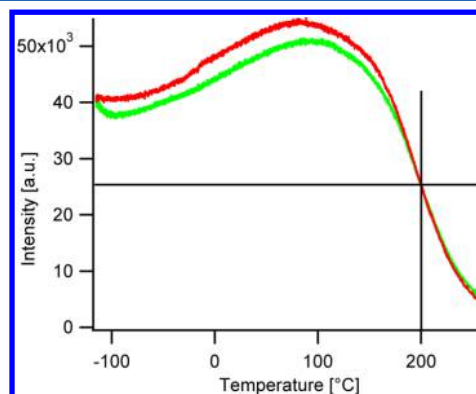
Figure 4. Emission intensity as a function of temperature of ordered $Ba_7F_{12}Cl_2$:Eu(0.89%). Heating (upper trace) and cooling (lower trace) experiments are shown.

integrated emission intensity (above 415 nm) upon excitation at 370 nm as a function of temperature between −100 and +250 °C. This experiment shows that the emission is not significantly quenched, at 200 °C about half the emission intensity is observed. This experiment is important, as the current near UV LED's still produce appreciable heat which can potentially quench the emission of the phosphor.

The decay of the $f-f$ lines is single exponential. The characteristic time for all the lines of the (A) group is 0.28(5) ms. The second group of lines (B) shows a longer lifetime (2.35(5) ms). The 80 and 10 K emission spectra show three $4f^6 5d \rightarrow 4f^7$ unresolved bands. The 5d component of the excited state is responsible for the strong electron vibration interaction which broadens the transition and forbids the observation of zero-phonon lines. The emission band at 23500 cm^{-1} (425 nm) resembles somewhat the emission band observed for Eu^{2+} in $Ba_{12}F_{19}Cl_5$,[17] which locally has similar Ba coordinations.[17,22] Each $f-d$ emission has an large Stokes-shift (≈ 8000 cm^{-1}). Two emission bands are shifted to the low energy side of the visible spectrum. Different mechanisms for such an emission displacement were proposed. In the oxides, CaO:Eu[23] and SrO:Eu,[24] the Stokes-shift is small and the red-shift of the emission was attributed to the covalency of host. The large Stokes-shift and the red displacement observed in BaF_2:Eu were assigned to an impurity trapped exciton.[25] Red shifts and large Stokes-shift of the Eu^{2+} emission in structures containing columns of alkaline earth ions were explained by a preferential orientation of an Eu^{2+} 5d orbital by the metal columns.[26−28] In $Ba_7F_{12}Cl_2$:Eu, large Stokes-shifts and columns of barium are present. Both mechanisms, the exciton and the preferential orientation of the 5d orbital, can explain the red-shift of the emission. Nevertheless, the large Stokes-shifts indicate that the excited state of Eu^{2+} is delocalized and couples strongly with the host crystal.

The millisecond decay of the narrow emission lines allows their assignment as $^6P_{7/2} \rightarrow {}^8S_{7/2}$ intra f-shell transitions.[29] Two different groups of $f-f$ transitions were observed (see Table 1). Each one corresponds to one type of Europium and has four lines due to the ligand field splitting of the $^6P_{7/2}$ level. Center B has a very large ligand field splitting of the $^6P_{7/2}$ level (198

cm^{-1}) in comparison with other Eu^{2+} doped halides.[19,29,30] As it is the case for the splitting of the $^8S_{7/2}$ ground-state (see the EPR results below), the large ligand field splitting is due to the high density of $Ba_7F_{12}Cl_2$ and to the low local symmetry of the Eu^{2+} sites. Lowering the temperature increases the f–f emission at the expense of the f–d ones for both sites. This shows that the $^6P_{7/2}$ levels of these two Eu^{2+} are at lower energy than the bottom of the $4f^65d^1$ structure.

As in many Eu^{2+}-doped halides,[31] the excitation spectrum is likely due to the lowest levels of the $4f^65d^1$ excited configuration. This structure is in part caused by the exchange interaction between the $4f^6$ and the $5d^1$. Another contribution to the overall structure comes from the quite important ligand field which affect more strongly the $4f^65d^1$ configuration than the $4f^7$ one.

Compared to the ordered form of $Ba_7F_{12}Cl_2$:Eu^{2+}, the disordered one exhibits a much less defined f–d emission pattern. Due to a distribution of different Eu^{2+} surroundings present in the structure, the emission spectrum of the disordered form consists of a superposition of bands impeding any meaningful assignment.

■ COLOR TUNING

Due to the presence of different Eu sites with different excitation spectra, the emission color can be tuned by choosing the excitation wavelength, as illustrated in Figure 5. The
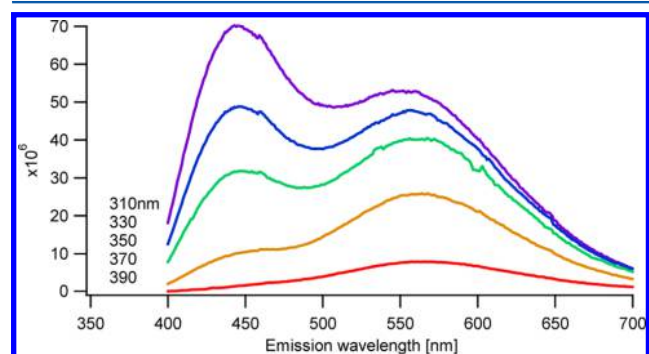
Figure 5. Emission spectra of disordered $Ba_7F_{12}Cl_2$:Eu^{2+} at different excitation wavelength (measured at 300 K).

increasing intensity with decreasing excitation wavelength reflects the excitation spectrum shown in Figure 1. Some of the resulting color temperatures are indicated in Table 2.

In order to evaluate the optimum Eu^{2+} concentration, samples of both ordered and disordered modifications were prepared with nominal Eu^{2+} concentrations of 0.1 to 10 mol % (with respect to Ba). The most intense emission was observed for the 3% doped sample; however, its intensity was only about 25% larger than the one doped with 1%. Figure 6 compares the emission spectra for the ordered samples excited at 337 nm. Note that crystal structure of single crystals isolated from the 10% sample were refined for the composition $Ba_6EuF_{12}Cl_2$.[28] With increasing Eu concentration, the blue emission band shifts to the red and its relative intensity decreases. This can be either explained by an increase of energy transfer between Eu ions in the crystal with increasing concentration (the lifetime measured at 450 nm is shorter than the one at 570 nm) and by a differentiated solubility of Eu^{2+} in the different Ba sites of the crystal. In the single crystal structure determination for

Table 2. Summary of Some Prototype Experiments

UV LED (nm)	sample	CIE coordinates	color temperature (K)	efficiency (lumen/W)
350	O[a]	0.2755, 0.3028	9762	n.d.
350	D[a]	0.3264, 0.3670	5733	n.d.
356	O[a]	0.2854, 0.3869	8361	n.d.
356	D[a]	0.3397, 0.3192	5270	n.d.
360	A[b]	0.311, 0.302	6899	89
	B[b]	0.310, 0.296	7066	171
375	A[b]	0.327, 0.316	5763	59
	B[b]	0.426, 0.530	3944	107
385	A[b]	0.401, 0.456	4519	29
	B[b]	0.366, 0.399	4011	66
395	A[b]	0.363, 0.39	4560	30
	B[b]	0.331, 0.323	5560	32

[a]The first four results were measured by the Swiss Federal Office for Weights and Measures (METAS) in Wabern/Berne on an ordered (O) and disordered (D) sample. [b]This work. Phosphor material $Ba_7F_{12}Cl_2$:Eu^{2+} (disordered modification). Sample A: 300 mg of 4.4% ethylcellulose + 95.6% xylene + 500 mg phosphor; sample B: 50% silicone paste (Invisil 4632A + Invisil 4632 B 1:1) + 50% phosphor.
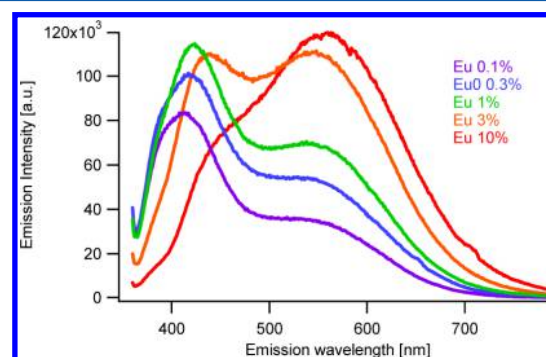
Figure 6. Room temperature emission spectra of ordered $Ba_7F_{12}Cl_2$ excited at 337 nm. The relative intensities have been arbitrarily normalized for clarity.

$Ba_6EuF_{12}Cl_2$,[32] Eu was located exclusively in the fluoride channels.

Modulation by Solid Solutions. It is possible to prepare solid solutions starting from $Ba_7F_{12}Cl_2$ in both ordered and disordered forms.[14−16] Figure S3 collects the lattice parameters of several compounds, which have been characterized by single crystal X-ray diffraction.

In this case, the emission spectra change only slightly: for instance, replacing Cl by Br leads to a blue shift of about 20 nm of the 590 nm band, while the blue band remains at practically the same position (see Figure S8).[15] The chemical substitutions (using Na, Mg, Ca, Sr, and Cl and Br) offer the possibility of fine-tuning the emission spectrum. More detailed studies (crystallographic and spectroscopic) on specific (different) individual mixed crystals are in progress.

■ EPR EXPERIMENTS

Most of the EPR spectra were recorded at 78 K; a few experiments were performed at 4.2 K to determine the absolute sign of the b_1^m parameters. Note that a typical spectrum of the Eu^{2+} ion consists of a pattern of seven groups of lines, as its

$^8S_{7/2}$ ground state is split by the ligand field and the hyperfine structure (^{151}Eu and ^{153}Eu, both $I = 5/2$).[33,34] But, in the present case, no resolved hyperfine structure was present. The spectra of two different Eu^{2+} EPR sites were observed in both the ordered and disordered form of Ba$_7$F$_{12}$Cl$_2$:Eu. Figure S9 shows recorded spectra of the two forms, obtained with the magnetic field **B** parallel to the a crystal axis. The labels (1) and (2) in Figure S9 mark those septets of each center, which show the largest respective splitting. The lines of the ordered form have a typical Full Width at Half Maximum (fwhm) of about 400 MHz and are about 500 MHz for the disordered form. Both forms of Ba$_7$F$_{12}$Cl$_2$:Eu show complex overall spectra, as the symmetry of these Eu^{2+} sites is lower than the factor group of the crystal. It was necessary to study the angular variations of the spectra in several crystallographic planes and with an angular increment of only 2.5°. Due to the small size of the single crystals studied, many accumulations were necessary to obtain an acceptable signal over noise ratio (S/N).

Ordered Form. The experimental angular variation of site No 1 obtained with **B** rotated in the (ab) plane is represented by the (+) symbols in Figure 7. It evidently reflects the
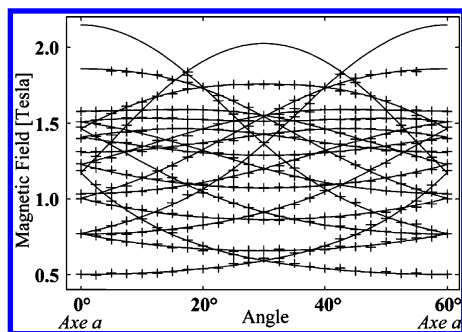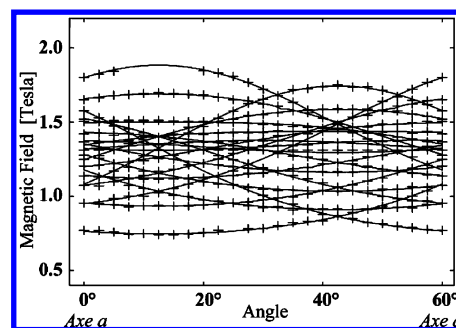

Figure 7. Experimental angular variation in the (ab) plane of the EPR spectrum No1 for the ordered Ba$_7$F$_{12}$Cl$_2$:Eu (crosses). The full lines represent the results of the simulation (see text; T = 78 K and v = 36.7 GHz).

hexagonal symmetry of the crystal. The angular variation within an (ac) plane proved that (ab) is a mirror plane. This applies for both sites. The site No. 1 presents a maximum fine structure splitting when **B** is parallel to the a axis. But the low S/N and the numerous overlapping lines do not allow to identify unambiguously the point group (D_{2h}, C_{2v}, C_{2h}, or C_s). The site symmetry of Ba(1) and Ba(2) is C_s.[12] The site No. 2 has its largest splitting at 15° from the a axis in the (ab) plane. Figure 8 shows the experimental angular variation in the (ab) plane for this site. The identification of the point group is not possible for the same reasons as mentioned above.

Disordered Form. The angular variations of the two paramagnetic centers in the disordered and ordered forms are similar. But the splittings between the lines and the orientation of the principal crystal field axis of the respective site 2 are clearly different. In the disordered form, the largest splitting is observed with the magnetic field along an a axis for site 1 and at 13° from an a axis for site 2. As is the case in the ordered form, (ab) is a mirror plane for the two sites and it is not possible to refine further the point group.

Parametrization. The procedure used to determine spin Hamiltonian parameters was already described elsewhere.[18,19] The angular variations of all sites were parametrized with the following spin Hamiltonian:

Figure 8. Experimental angular variation in the (ab) plane of the EPR spectrum No2 for the ordered Ba$_7$F$_{12}$Cl$_2$:Eu (crosses). The full lines represent the results of the simulation (see text; T = 78 K and v = 36.7 GHz).

$$\mathbf{H} = g\beta_0\mathbf{B}\cdot\mathbf{S} + (b_2^0 O_2^0 + b_2^2 O_2^2) \tag{1}$$

where the O_2^0 and O_2^2 represent Steven's operator equivalents.[33,34] The other symbols have their usual meaning. Formally, the O_4^m and O_6^m terms of appropriate symmetry have to be included. But as the spectral components have typical fwhm larger than 400 MHz, a residual error of approximately 160 MHz/point was already attained by fitting this equation to the angular variations. The inclusion of the other terms resulted in marginal improvement of the fit. It is often observed that the b_2^0 and b_2^2 parameters are the most important ones to parametrize angular variations of low symmetry situations.[18,21,35] The optimized parameters for all sites are given in Table 3. The indicated errors correspond to

Table 3. Spin Hamiltonian Parameters for Eu^{2+} in Two Sites in Ordered (O) and Disordered (D) Ba$_7$F$_{12}$Cl$_2$[a]

site	b_2^0 (10^{-4} cm^{-1})	b_2^2 (10^{-4} cm^{-1})	angle	splitting (cm^{-1})
O1	392 ± 9	−328 ± 20	0° ± 2	1.64
O2	−297 ± 8	67 ± 17	15° ± 2	1.09
D1	428 ± 8	−289 ± 16	0° ± 2	1.72
D2	−294 ± 7	141 ± 18	13° ± 2	1.13

[a]For all four spectra, g = 1.99(1).

the variation needed to double the residual error of the fits. The absolute sign of the crystal field parameters was determined by analyzing the relative intensities at 4.2 K. Theoretical angular variations calculated with the aid of the constants of Table 3 are shown as full lines in Figures 5 and 6.

Eu^{2+} ions occupy the Barium lattice sites in many Barium halides and related compounds, in agreement with isocharge arguments. This was demonstrated in barium halides with the aid of EPR[18,21,35,36] and by X-ray diffraction of highly doped crystals.[32,37,38] Table S1 lists spin Hamiltonian parameters of Eu^{2+} in different barium fluorohalides. Three different barium sites (of point symmetry m, m and C_{3h}) are present in the ordered Ba$_7$F$_{12}$Cl$_2$ structure. But the EPR results show only two different Eu^{2+} ions, both of low symmetry. No hexagonal spectrum was found. X-ray diffraction of Ba$_7$F$_{12}$Cl$_2$ heavily doped with Europium has, however, shown that europium substitutes barium at this site.[32] To explain the absence of hexagonal EPR spectra, the following reasons are considered.

We assume equal probabilities for the Eu^{2+} to substitute any of the three sites. The low symmetry part of the EPR spectrum is produced by 2 × 3 Eu^{2+} over the ensemble of the unit cells involved, whereas only one Eu^{2+} is expected to generate a

hexagonal one. The many wide EPR lines of the low symmetry centers produce important overlaps which may strongly complicate the identification of the weak third center.

Another argument comes from X-ray diffraction results in conjunction with considerations regarding the structure of eq 1. X-ray diffraction[32] showed a large vibration ellipsoid along the c axis for the hexagonal Eu^{2+} in highly doped crystals The possibility of Eu^{2+} moving in a double-well along c has thus to be considered, in agreement with ionic radius arguments (the ionic radius of Eu^{2+} is smaller than the one of Ba^{2+}). The local symmetry of the Eu^{2+} is C_{3h} on the hexagonal lattice site, but it is C_3 when shifted along the c axis. In the former situation the crystal field part of eq 1 contains U_2^0, U_4^0, U_6^0 ($U_6^6 + U_6^{-6}$), whereas the symmetry C_3 includes in addition the terms ($U_4^3 -$ U_4^{-3}), ($U_6^3 - U_6^{-3}$) (we set $U_n^m = b_n^m * O_n^m$). In the event that Eu^{2+} switches through thermal activation between the two wells with a jump rate of the order of the EPR microwave frequency, these additional terms become time-dependent perturbations. Such a dynamic process could broaden and weaken the EPR lines, making their identification more difficult.

The third possibility takes into account the tendency for local disorder (again related to the different ionic radii) which is at the origin of the large inhomogeneous width of the low symmetry EPR lines. The Eu^{2+} concentration is nominally 0.4% and no pair EPR was observed. Statistically the Eu^{2+} ions are thus mutually well separated. If part (or all) of this ion shift in the mirror-plane away from C_6 and form with their fluorine neighbors a local cluster of symmetry m, their EPR spectrum will be of the same symmetry as the one of the sites 1 and 2. Due to the strong inhomogeneous broadening, the resulting EPR spectrum will consist of large lines with unresolved fine structure and an intensity 1/7 (see above). Again, but of course not for the same reasons, their identification would be difficult. Endor experiments might be appropriate in this situation. An interpretation along this line would reconcile rather coherently the different experimental results reported here.

The spin Hamiltonian parameters of Table 3 allow to calculate the ligand field splitting in the ground state. The total splitting for the four EPR centers are given in Table 3. All of them are larger than 1 cm^{-1}. Such splittings are very large for the ground state of Eu^{2+} in halides.[18,19] This is due to the high density of the $Ba_7F_{12}Cl_2$, which causes short distances between the Eu^{2+} and their ligands.[12] The low symmetry of the Eu^{2+} sites also contributes to enlarge the splitting by preventing partial compensation between individual ligand contributions, as is the case in $BaFCl$.[39]

POTENTIAL DEVICE TESTING

Pellets of Ba7(o) (sample 8170, nominally 1.1% Eu^{2+}) and Ba7(d) (sample 8172) were submitted to the Swiss Federal Office for Weights and Measures (METAS) in Wabern/Berne for the determination of the color temperature and coordinates (at excitation wavelengths 350 and 356 nm).

Further experiments were done with the setup illustrated in Figure S4 on powders of disordered $Ba_7F_{12}Cl_2$ mixed with a binder. The powder was obtained by manual grinding in an agate mortar, the particle size and size distribution were not measured. This sample was chosen as it emits a rather warm white (color temperature 4000−7000 K). The results of the tests are summarized in Table 2. The near-UV LEDs used were emitting at 360, 375, 385, and 395 nm. The highest efficiency was obtained using the 360 nm LED emission, with 171 lm/W (light to light conversion). A commercial phosphor should have

about 3 times this value. Considering that the ordered modification has a stronger absorption in the near UV than the disordered modification, as well as the fact that our sample was manually ground and may thus not have an optimal grain size and grain size distribution, there appears to be room for improvement. This sample has also a good CRI of 83. With increasing wavelength, the efficiency decreases, which can be related to the decreasing absorption coefficient as seen also in the excitation spectrum of Figure 1. The CIE color coordinates confirm that all compounds have practically white emission with coordinates rather close to the ideal value of x,y = 0.333,0.333. The table shows also the change of color temperature with changing wavelength, ranging from 3944 to 9762 K. Typically, with increasing wavelength (with the exception of the values at 395 nm), the color temperature decreases, in agreement with the emission spectra shown above (Figure 3).

CONCLUSIONS

The phosphor $Ba_7F_{12}Cl_2{:}Eu^{2+}$ presents a broad emission spectrum in the visible that can be excited by near UV illumination. The substitution of Ba^{2+} by Eu^{2+} on three different lattice sites (for the ordered modification) leads to the superposition of three emission spectra which covers large parts of the visible spectrum. This crystallochemical property is the key to obtain a single compound phosphor material. The superposition of different emission spectra also allows to tune the emission color with the excitation wavelength, as the excitation spectra are inherently different. The EPR spectra show two different sites with significantly different zero field splitting which can be assigned to the Ba(1) and Ba(2) sites of the crystal. This can also be associated with the observation of relatively well separated emission bands (at 425 and 500 nm). The nonobservation of the third EPR spectrum suggests that the electronic degeneracy in the excited $4f^5 5d^1$ energy level structure is lifted and possibly associated with a Jahn−Teller or pseudo Jahn−Teller effect.

The emission properties can be tuned chemically by choosing one of the two crystal modifications, partial replacement of Ba by other ions, substitution of chloride by bromide as well as dopant Eu-ion concentration. Furthermore, the emission can also be tuned by the choice of excitation wavelength. Prototype tests with UV LEDs as excitation source show good UV to visible conversion efficiencies and also good CRI, which show good promise for illumination applications. However, the presently available UV LEDs show very poor efficiencies of conversion of electric into UV energy, which is currently the major impediment for commercial lighting applications.

The concept of making a dedicated crystallochemical search for host materials with significantly different sites for the same constituent (in our case Ba) will allow to prepare new interesting phosphors in the future.

ASSOCIATED CONTENT

ⓢ Supporting Information

Drawings of the crystal structures, illustration of crystal growth furnace, lattice parameters for partially substituted compounds, additional spectra, device testing setup, and report of the Swiss Federal Office for Weights and Measures. This material is available free of charge via the Internet at http://pubs.acs.org.

146

dx.doi.org/10.1021/jp510301p | J. Phys. Chem. C 2015, 119, 141−147

■ AUTHOR INFORMATION

Corresponding Author

*Phone + 41 22 3796539. E-mail: hans-rudolf.hagemann@unige.ch.

Present Address

‡ZHAW, Zurich University of Applied Sciences IAMP, Institute of Applied Mathematics and Physics TP213, Technikumsstrasse 9 8401 Winterthur; E-mail: julien.rey@zhaw.ch (J.M.R.).

Notes

The authors declare no competing financial interest.

■ REFERENCES

(1) Tsao, J. Y. *Light Emitting Diodes (LEDs) for General Illumination*; Optoelectronics Industry Development Association: Washington, DC, 2002.

(2) D'Andrade, B. W.; Forrest, S. R. White Organic Light Emitting Devices for Solid State Lighting. *Adv. Mater.* **2004**, *16*, 1585−1595.

(3) Wen, Y.; Wang, Y.; Zhang, F.; Liu, B. Near Ultraviolet Excitable $Ca_4Y_6(SiO_4)_6O:Ce^{3+},Tb^{3+}$ White Phosphors for Light-Emitting Diodes. *Mater. Chem. Phys.* **2011**, *129*, 1171−1175.

(4) Guo, N.; Zheng, Y.; Jia, Y.; Qiao, H.; You, H. Warm-White-Emitting from Eu^{2+}/Mn^{2+}-Codoped $Sr_3Lu(PO_4)_3$ Phosphor with Tunable Color Tone and Correlated Color Temperature. *J. Phys. Chem. C* **2012**, *116*, 1329−1334.

(5) Yan Chen, Y. L.; Wang, J.; Wu, M.; Wang, C. Color-Tunable Phosphor of Eu^{2+} and Mn^{2+} Codoped $Ca_2Sr(PO_4)_2$ for UV Light-Emitting Diodes. *J. Phys. Chem. C* **2014**, *118*, 12494−12499.

(6) Chien-Hao, H.; Wei-Ren, L.; Teng-Ming, C. Single-Phased White-Light Phosphors $Ca_9Gd(PO_4)_7:Eu^{2+},Mn^{2+}$ under Near-Ultraviolet Excitation. *J. Phys. Chem. C* **2010**, *114*, 18698−18701.

(7) Sai, Q.; Xia, C.; Rao, H.; Xu, X.; Zhou, G.; Xu, P. Mn, Cr-Co-Doped $MgAl_2O_4$ Phosphors for White LEDs. *J. Lumin.* **2011**, *131*, 2359−2364.

(8) Dorman, J. A.; Choi, J. H.; Kuzmanich, G.; Chang, J. P. High Quality White Light Using Core-Shell $RE^{3+}:LaPO_4$ (RE = Eu, Tb, Dy, Ce) Phosphors. *J. Phys. Chem. C* **2012**, *116*, 12854−12860.

(9) Lorbeer, C.; Mudring, A.-V. White-Light-Emitting Single Phosphors Via Triply Doped LaF_3 Nanoparticles. *J. Phys. Chem. C* **2013**, *117*, 12229−12238.

(10) Chien-Hao, H.; Teng-Ming, C. A Novel Single-Composition Trichromatic White-Light $Ca_3Y(GaO)_3(BO_3)_4:Ce^{3+},Mn^{2+},Tb^{3+}$ Phosphor for UV-Light Emitting Diodes. *J. Phys. Chem. C* **2011**, *115*, 2349−2355.

(11) Bill, H.; Hagemann, H.; Kubel, F. Discharge electric lamp. *PCT Int. Appl WO 99 17,340 (Cl H01J61/44)*, 8 Apr 1999, CH Appl. 97/2,277, 29 Sep 1997.

(12) Kubel, F.; Bill, H.; Hagemann, H. Synthesis and Structure of $Ba_7F_{12}Cl_2$. *Z. Anorg. Allg. Chem.* **1999**, *625*, 643−649.

(13) Kubel, F.; Hagemann, H. On the Crystallochemical Origin of the Disordered Form of $Ba_7^{(EuII)}F_{12}Cl_2$ and the Structural Changes Induced at High Temperature. *Cryst. Res. Technol.* **2006**, *41*, 1005−1012.

(14) Frühmann, B.; Kubel, F.; Hagemann, H.; Bill, H. Synthesis and Structure of the New Fluoride Bromide $Ba_{6.668(2)}Ca_{0.332(2)}F_{12}Br_2$ and Solid Solutions with Composition $Ba_{7-x}Ca_xF_{12}(Cl_yBr_{1-y})_2$ with $x = 0.5$, $0 < y < 1$. *Z. Anorg. Allg. Chem.* **2004**, *630*, 1484−1488.

(15) Penhouet, T.; Hagemann, H.; Kubel, F.; Rief, A. Calcium-Free Solid Solutions in the System $Ba_7F_{12}Cl_{2-x}Br_x$ ($x < 1.5$), a Single-Component White Phosphor Host. *J. Chem. Cryst.* **2007**, *37*, 469−472.

(16) Hagemann, H.; Penhouet, T.; Rief, A.; Kubel, F. Crystallochemical Studies in the Family of Crystals $Ba_{7-x}Na_yF_{12}Cl_{2-z}Br_z$ ($x < 0.1$, $y < 0.2$, $z < 1.5$). *Z. Anorg. Allg. Chem.* **2008**, *634*, 1041−1044.

(17) Hagemann, H.; D'Anna, V.; Lawson Daku, M.; Kubel, F. Crystal Chemistry in the Barium Fluoride Chloride System. *Cryst. Growth Des.* **2012**, *12*, 1124−1131.

(18) Rey, J. M.; Bill, H.; Lovy, D.; Hagemann, H. Europium Doped $BaMgF_4$, an EPR and Optical Investigation. *J. Alloys Comp.* **1998**, *268*, 60−65.

(19) Rey, J. M., *Ph.D. Thesis, No. 3189*, Univ. of Geneva, 2000.

(20) Antic-Findancev, E.; Lemaitre-Blaise, M.; Caro, P. Crystal Field Splitting of Gadolinium ($4f^7$) Levels in C-Type Rare Earth Oxides. *J. Chem. Phys.* **1982**, *76*, 2906−2913.

(21) Rey, J. M.; Bill, H.; Lovy, D.; Kubel, F. EPR and Optical Investigation of Europium Doped $Ba_{12}F_{19}Cl_5$. *J. Phys.: Condens. Matter* **1999**, *11*, 7301−7309.

(22) Kubel, F.; Hagemann, H.; Bill, H. Synthesis and Structure of $Ba_{12}F_{19}Cl_5$. *Z. Anorg. Allg. Chem.* **1996**, *622*, 343−347.

(23) Yamashita, N. Coexistence of the Eu^{2+} and Eu^{3+} Centers in the CaO:Eu Powder Phosphor. *J. Electrochem. Soc.* **1993**, *140*, 840−843.

(24) Yamashita, N. Photoluminescence Spectra of the Eu^{2+} Center in SrO:Eu. *J. Lumin.* **1994**, *59*, 195−199.

(25) Moine, B.; Courtois, B.; Pedrini, C. Photoionization and Luminescences in $BaF_2:Eu^{2+}$. *J. Lumin.* **1991**, *50*, 31−38.

(26) Poort, S. H. M.; Blokpoel, W. P.; Blasse, G. Luminescence of Eu^{2+} in Barium and Strontium Aluminate and Gallate. *Chem. Mater.* **1995**, *7*, 1547−1551.

(27) Poort, S. H. M.; van Krevel, J. W. H.; Stomphorst, R.; Vink, A. P.; Blasse, G. Luminescence of Eu^{2+} in Host Lattices with Three Alkaline Earth Ions in a Row. *J. Solid State Chem.* **1996**, *122*, 432−435.

(28) Poort, S. H. M.; Janssen, W.; Blasse, G. Optical Properties of Eu^{2+}-Activated Orthosilicates and Orthophosphates. *J. Alloys Comp.* **1997**, *260*, 93−97.

(29) Hewes, R. A.; Hoffman, M. V. $4f^7$-$4f^7$ Emission for Eu^{2+} in the System $MF_2 \cdot AlF_3$. *J. Lumin.* **1971**, *3*, 261−280.

(30) Sytsma, J.; Blasse, G. Comparison of the Emission of Eu^{2+} in MFCl (M = Sr, Ba) and of Gd^{3+} in YOCl. *J. Lumin.* **1992**, *51*, 283−292.

(31) Rubio, J. Doubly-Valent Rare-Earth Ions in Halide Crystals. *J. Phys. Chem. Solids* **1991**, *52*, 101−174.

(32) Kubel, F.; Bill, H.; Hagemann, H. Synthesis and Structure of the Ordered Modification of $Ba_6EuF_{12}Cl_2$. *Z. Anorg. Allg. Chem.* **2000**, *626*, 1721−1722.

(33) Stevens, K. W. H. Matrix Elements and Operator Equivalents Connected with the Magnetic Properties of Rare Earth Ions. *Proc. Phys. Soc.* **1952**, *65*, 209−215.

(34) Abragam, A.; Bleaney, B. *Electron Paramagnetic Resonance of Transition Ions*; Clarendon Press: Oxford, 1970.

(35) Rey, J. M.; Bill, H.; Lovy, D.; Hagemann, H. EPR and Optical Investigation of Europium Doped $Ba_2Mg_3F_{10}$. *J. Alloys Comp.* **1998**, *274*, 164−168.

(36) Nicollin, D.; Bill, H. Gd^{3+}, Eu^{2+} in SrFCl and BaFCl Single Crystals: EPR Results. *Solid State Commun.* **1976**, *20*, 135−137.

(37) Kubel, F.; Hagemann, H.; Bill, H. Crystal Structures of Eu(II) Substituted Barium Magnesium Fluorides: $Ba_{0.78(3)}Eu_{0.22(3)}MgF_4$ and $Ba_{5.20(6)}Eu_{0.80(6)}Mg_7F_{26}$. *Z. Kristallogr.* **1999**, *214*, 139−142.

(38) Reckeweg, O.; DiSalvo, F. J.; Wolf, S.; Schleid, T. Two Ternary Mixed-Anion Chlorides with Divalent Europium: Eu_2H_3Cl and $Eu_7F_{12}Cl_2$. *Z. Anorg. Allg. Chem.* **2014**, *640*, 1254−1259.

(39) Nicollin, D.; Bill, H. Experimental Contribution to the Study of S-State Ions in Ionic Single Crystals. *J. Phys. C* **1978**, *11*, 4803−4814.